npj | vaccines

Article

Published in partnership with the Sealy Institute for Vaccine Sciences

https://doi.org/10.1038/s41541-025-01155-4

An RBD-Fc mucosal vaccine provides variant-proof protection against SARS-CoV-2 in mice and hamsters

Yanjun Zhang[1,2,8], Yan Wu[3,8], Meng-Qian Zhang[4,8], Haiyue Rao[1,8], Zhaoyong Zhang[1,8], Xiangyue He[1,8], Yiwen Liang[1], Raoqing Guo[1], Yaochang Yuan[1], Jing Sun[1], Helen M. E. Duyvesteyn[5], Elizabeth E. Fry[5], David I. Stuart[5,6,7], Jingxian Zhao[1,2], XiaoYan Pan[3] ✉, Shu-Lin Liu[4] ✉, Jincun Zhao[1,2] ✉ & Jiandong Huo[1,2] ✉

Current severe acute respiratory syndrome coronavirus 2 (SARS-CoV-2) vaccines are effective against severe disease and death, but do not prevent viral infections, probably due to the limited mucosal immunity induced by intramuscular administration of the vaccine. Fusion of SARS-CoV-2 subunit immunogens with a human IgG Fc backbone can be used as a mucosal vaccine but its effectiveness in delivery in animal models, and its immunogenicity and the vaccine-induced protection against viral infections requires further studies. Here we investigate a bivalent RBD-Fc vaccine that includes the spike receptor-binding domains (RBDs) of the ancestral and BQ.1.1 variant of SARS-CoV-2. Ex vivo fluorescent imaging demonstrates that this vaccine can be effectively delivered to the lungs of mice through intranasal administration, with enhancement of retention in the nasal cavity and lung parenchyma. In mice, the vaccine elicited potent and broad-spectrum antibody responses against different variants including KP.3 which could persist for at least 3 months after booster. Importantly, it was able to induce RBD-specific mucosal IgA responses. Further, heterologous intranasal immunisation with adeno-vectored Chadv1 and RBD-Fc elicited both potent neutralising antibody and T cell responses. Immunised BALB/c and K18-hACE2-transgenic mice were also protected against viral challenge of XBB.1 and viral transmission was effectively limited in hamsters through intranasal immunisation. This work thus demonstrates the potential of RBD-Fc antigens as mucosal vaccines for prevention of breakthrough infections and onward transmission. Moreover, Fc-fusion proteins can be used as an effective mucosal vaccine strategy which can be used either alone or in combination with other vaccine technology to constitute heterologous immunisations, enabling strong protection against SARS-CoV-2 and other respiratory viruses.

The global pandemic of coronavirus disease 2019 (COVID-19) has entered the fifth year since the emergence of severe acute respiratory syndrome coronavirus 2 (SARS-CoV-2) in late 2019. Although COVID-19 vaccines became available with an unprecedented speed of just one year after identification of the pathogen[1,2], they are more effective at reducing the risk of hospitalization and death than transmission[3,4]. Notably, since the Omicron variant, bearing a large number of receptor binding domain (RBD) mutations, emerged in November 2021[5], a number subvariants have emerged showing greater transmissibility and antibody escape capacity, including BQ.1.1, XBB.1, EG.5, BA.2.86 and JN.1[6,7], causing breakthrough infections,

[1]State Key Laboratory of Respiratory Disease, National Clinical Research Center for Respiratory Disease, Guangzhou Institute of Respiratory Health, the First Affiliated Hospital of Guangzhou Medical University, Guangzhou, China. [2]Guangzhou National Laboratory, Bio-island, Guangzhou, China. [3]State Key Laboratory of Virology and Biosafety, Wuhan Institute of Virology, Chinese Academy of Sciences, Beijing, China. [4]State Key Laboratory of Medicinal Chemical Biology, TianjinKey Laboratory of Biosensing and Molecular Recognition,Frontiers Science Centre for New Organic Matter, ResearchCentre for Analytical Sciences, College of Chemistry, Nankai University, Tianjin, PR China. [5]Division of Structural Biology, Nuffield Department of Medicine, University of Oxford, The Wellcome Centre for Human Genetics, Oxford, UK. [6]Chinese Academy of Medical Science (CAMS) Oxford Institute (COI), University of Oxford, Oxford, UK. [7]Diamond Light Source Ltd, Harwell Science & Innovation Campus, Didcot, UK. [8]These authors contributed equally: Yanjun Zhang, Yan Wu, Meng-Qian Zhang, Haiyue Rao, Zhaoyong Zhang, Xiangyue He. ✉e-mail: panxy@wh.iov.cn; shulin.liu@nankai.edu.cn; zhaojincun@gird.cn; huojiandong@gird.cn

regardless of vaccine type or vaccination strategy[8–10]. Despite the high coverage of vaccination in most countries, the number of COVID-19 cases reported to WHO is rising at a rate of over 40,000/week as of August 2024 (https://covid19.who.int/), which might be underestimated as milder and asymptomatic cases are less likely to be captured by surveillance systems. Although new variants of SARS-CoV-2 such as JN.1 may be associated with a lower risk of severe disease compared to previous predominant variants, they can still cause typical COVID-19 symptoms and lead to severe disease and death[11,12]. Moreover, even if many infected individuals had only mild symptoms, it is estimated that around 10–20% of convalescents may experience persistent symptoms, known as post-COVID-19 syndrome or long COVID (WHO post COVID-19 condition). Many diseases can be caused or made worse by long COVID, including cardiovascular and cerebrovascular diseases, type 2 diabetes and autoimmune diseases, leaving a significant proportion of people unable to return to work[13]. Therefore, COVID-19 remains a dangerous infectious disease, still poses a substantial threat to health and health systems and there is an urgent need for more effective vaccines and better vaccination coverage.

Breakthrough infections have been commonly observed for vaccinated individuals, especially 3 months post-immunisation[14]. which is partly due to the increasing humoral escape capacity of the emerging variants, and waning of systemic humoral responses[15], In addition, intramuscular vaccine administration induces a poor mucosal immunity[16,17] that is considered to play an important role in protecting against SARS-CoV-2 infection at the route of entry[18]. By contrast, delivery of immunogens through the mucosal surface could be an efficient approach for eliciting potent mucosal immunity against SARS-CoV-2 infections. As adenoviruses naturally infect through mucosal surfaces, adenoviral-vectored vaccines have been favoured for mucosal vaccination. However, in addition to the potential serious adverse event of vaccine-induced thrombosis with thrombocytopenia syndrome (TTS) that has been observed following intramuscular vaccination with adenovirus vector COVID-19 vaccines (ChAdOx1-S and Ad26.COV2.S)[19], clinical trial data of intranasal vaccination with adenoviral-vectored vaccines are unsatisfactory, failing to elicit adequate immune response in healthy volunteers, despite of various successes in preclinical studies[20], thus suggesting the urgent need to investigate other technologies that are suitable for mucosal vaccination.

While the mucosal surfaces are impervious to diffusion of macromolecules, the neonatal receptor for the Fc fragment of immunoglobulin G (FcRn) expressed in the nasal airway and the olfactory epithelium allows transport of IgG and IgG Fc-containing molecules across the airway mucosal barrier[21]. A previous study showed that immunisation of an IgG Fc fusion of herpes simplex virus type-2 (HSV-2) glycoprotein gD together with a CpG adjuvant was able to elicit robust mucosal and systemic immune responses, providing complete protection against viral challenge in a FcRn-dependent manner[22]. Compared to monovalent immunogens, bivalent Fc-linked immunogens may be able to elicit more robust B-cell responses by triggering cross-linking of B-cell receptors[23].

The RBD of the SARS-CoV-2 spike (S) is an ideal immunogen to be presented by the IgG Fc. RBD mediates the binding of S protein to the host cellular receptor angiotensin converting enzyme 2 (ACE2) receptor, thus initiating viral entry[24]. RBD is highly immunogenic, and to date, the majority of characterised potently neutralising antibodies (NAbs) are against the RBD. Most of these function by blocking receptor binding[25–28], but some seem to neutralise by destabilising the trimeric S[29,30]. Moreover, as the mutations of emerging variants primarily occur at the RBD[31], linking RBD from an ancestral (referred as WT in the rest of the text) strain and a dominant strain to form a bivalent vaccine can overcome the immune evasion capacity acquired by the new variants.

Previously, we showed that induction of cross-reactive RBD-specific B cell response which can overcome viral immune escape, can be promoted by co-displaying SARS-CoV-2 WT RBD and SARS-CoV RBD which are antigenically distant while partially conserved antigens[32]. Here, we constructed a bivalent RBD-Fc vaccine containing the RBD of SARS-CoV-2 WT strain and BQ.1.1 strain, whose antigenic distance is suggested to be similar to that of the SARS-CoV-2 WT stain and SARS-CoV, which are linked to an engineered human IgG4 Fc backbone. We evaluated the efficacy of intranasal (IN) delivery of this vaccine and its immunogenicity in mouse models, as well as its capacity to limit viral transmission in a hamster model. We also explored the potential of heterologous vaccination with a SARS-CoV-2 spike-based adenoviral vector vaccine following a booster with our RBD-Fc vaccine to elicit strong B-cell and T-cell responses. Our results show that this may be a useful mucosal vaccine design strategy for the control of SARS-CoV-2 and possibly other respiratory viral infections, either used as homologous or heterologous mucosal vaccination strategies.

Results

Construction, purification and characterisation of bivalent SARS-CoV-2 RBD-Fc recombinant proteins

To generate the construct encoding the bivalent WT-BQ.1.1 RBD-Fc (referred as RBD-Fc in the rest of the text), we first modified the Fc fragment of human IgG4, with the introduction of following mutations: S228P to stabilize the Fc, F234A + L235A to silence effector function, R409K to reduce aggregation, and K447del to reduce C-terminal heterogeneity. An Fc fragment of human IgG4 was chosen because ACE2, the receptor for RBD, is ubiquitously expressed in a wide range of cells including heart, lung, kidney and brain; IgG4 only weakly activates antibody-dependent immune effector responses; and the use of modified IgG4 Fc with F234A + L235A mutations can avoid host cell damage potentially caused by immunisation with an Fc vaccine, avoiding inflammatory responses and discomfort resulting from vaccination. To overcome the antibody evasion by new SARS-CoV-2 variants, RBD (333-529 aa) from the ancestral strain (referred as WT herein) and BQ.1.1 variant (the dominant strain at the time of this work started) were joined together with a flexible $(GGGGS)_3$ linker and fused to the modified IgG4 Fc (Fig. 1a). The RBD-Fc construct was expressed using mammalian (Freestyle 293 F) cells, and the recombinant protein purified using Immobilized-metal affinity chromatography followed by a size exclusion chromatography, and Coomassie blue staining of the SDS-PAGE gel revealed a single band; the size of the RBD-Fc protein in the non-reducing condition was 2-times of that in the reducing condition as RBD-Fc forms a dimer through disulphide bonds between the Fc region under the non-reducing condition (Fig. 1b). The purity of the bivalent RBD and RBD-Fc was demonstrated by size exclusion chromatography, in both cases, the protein ran as a single peak (Fig. 1c).

Superior nasal and lung biodistribution and retention of RBD-Fc over RBD

To investigate the nasal and lung biodistribution and retention of the RBD-Fc vaccine, equal molar concentration of RBD-Fc or RBD (0.2 nM) conjugated with a Cy5 NHS Ester far-red-fluorescent dye were intranasally administered to mice. A bivalent RBD was used as a control as it is a comparable protein subunit that is small enough for intranasal delivery despite lacking an Fc region. Nasal cavity (Fig. 1d, e), e*x vivo* imaging analysis showed that a comparable amount of RBD-Fc and RBD was detected at 4 h post administration, however the RBD signal decreased rapidly over time, so that significantly more RBD-Fc was present at both 24 h and 48 h time points. Substantially more RBD-Fc than RBD was able to reach and retain in the lungs (Fig. 1f, g), and this superiority was maintained over time. While RBD-Fc was retained for over 72 h, hardly any RBD was detected at 48 h.

RBD-Fc vaccine elicited robust and durable antibody responses in BALB/c mice

To evaluate the immunogenicity of the RBD-Fc vaccine, 6–8-week-old female BALB/c mice were immunised twice intramuscularly (IM, with a Sigma Adjuvant System / SAS adjuvant) or intranasally (IN, with and without CpG ODN, a potent adjuvant for the induction of mucosal immune response[33]) administered at a 4-week interval (Fig. 2a), and the mice were bled on 7 days and 28 days post-booster to evaluate the serum neutralisation titres. In addition to finding out whether adding a CpG adjuvant can

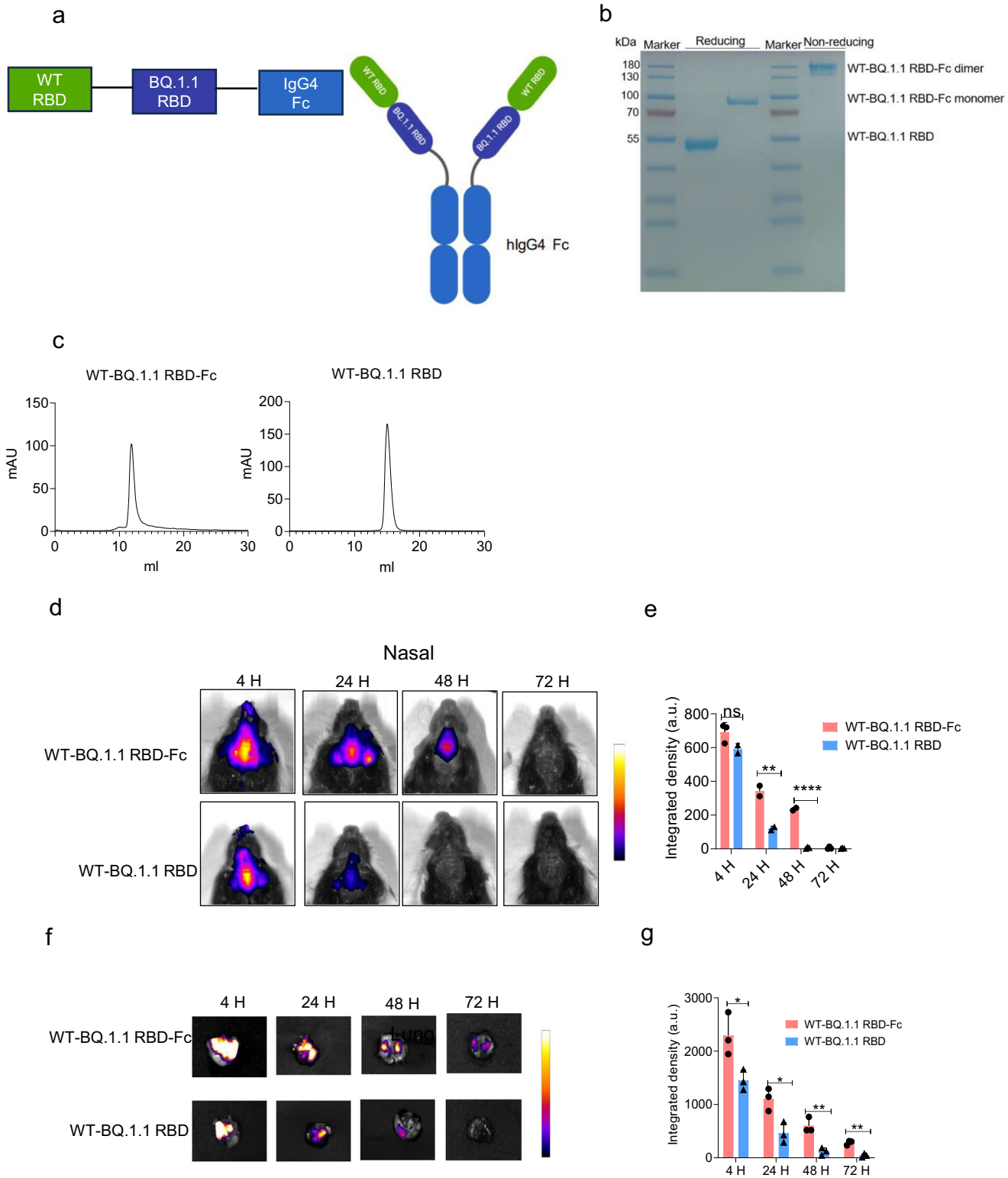

Fig. 1 | Characterization of WT-BQ.1.1 RBD-Fc and tissue distribution of the WT-BQ.1.1 RBD-Fc. a Schematic of WT-BQ.1.1 RBD-Fc: WT and BQ.1.1 RBD of SARS-CoV-2 linked with GS and fused to the N-terminal of the IgG4 Fc. **b** SDS-PAGE/commissa blue staining of WT-BQ.1.1 RBD-Fc, WT-BQ.1.1 RBD under reducing and non-reducing conditions. **c** Gel filtration chromatograms of the WT-BQ.1.1 RBD-Fc and WT-BQ.1.1 RBD. **d** Ex vivo imaging of mouse nasal after Cy5-loaded WT-BQ.1.1 RBD-Fc or Cy5-loaded WT-BQ.1.1 RBD delivery after 4 h, 24 h, 48 h, 72 h. **e** Quantification of the integrated density of Cy5 fluorescence in ex vivo mouse nasal; each dot represents data from one lung, $n = 3$ per group. **f** Ex vivo imaging of mouse lungs after Cy5-loaded WT-BQ.1.1 RBD-Fc or Cy5-loaded WT-BQ.1.1 RBD delivery after 4 h, 24 h, 48 h, 72 h. **g** Quantification of the integrated density of Cy5 fluorescence in ex vivo mouse lungs; each dot represents data from one lung, $n = 3$ per group.

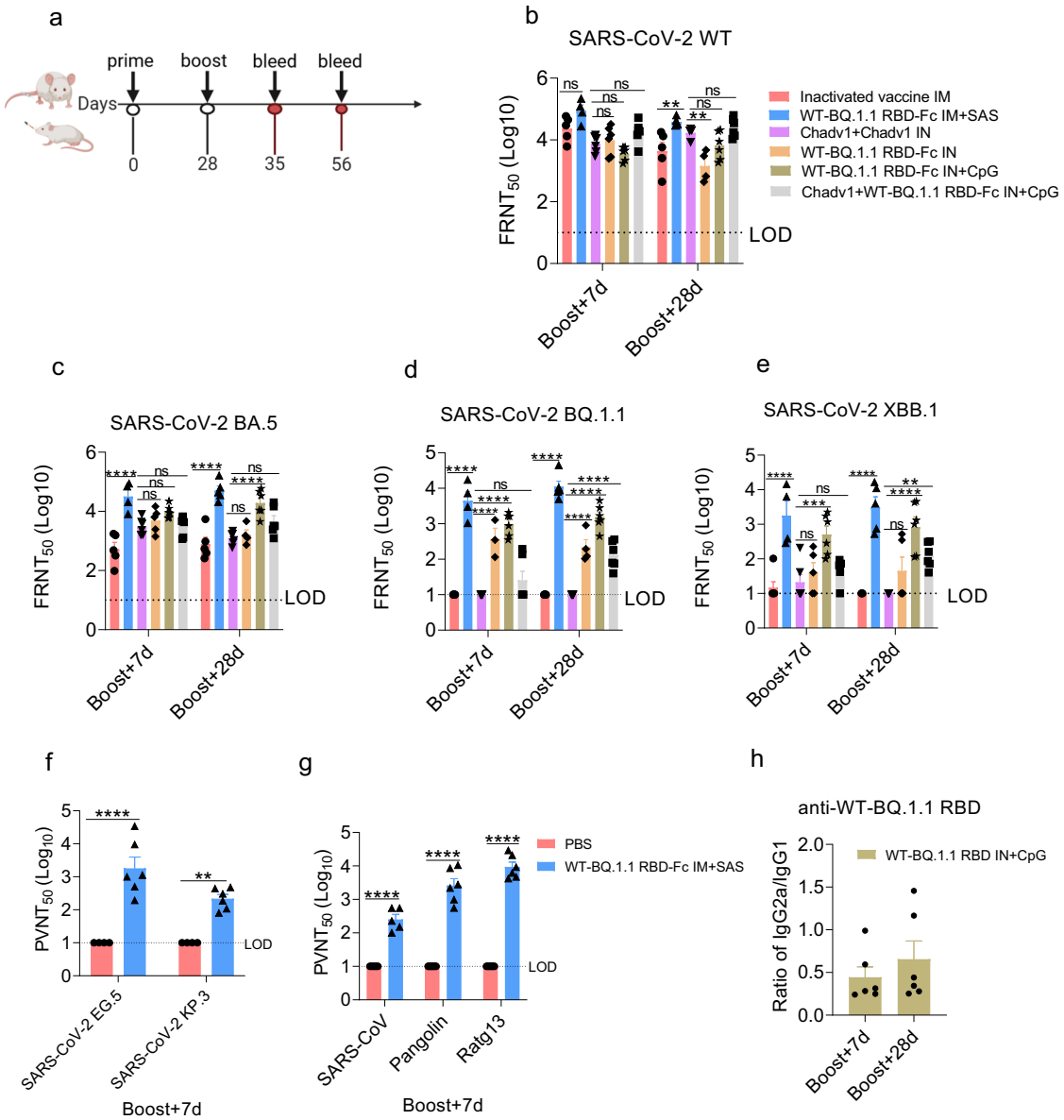

Fig. 2 | Immunisation of WT-BQ.1.1 RBD-Fc induce robust humoral response in mice. a Scheme of the immunisation process in mice. **b** Six-week-old female BALB/c mice were immunised with different vaccine. Mice were boosted 4 weeks with homologous or heterologous antigen dose after primary vaccination. Sera were collected at 7 and 28 days after the boosted immunisation. Neutralization antibody titre of SARS-CoV-2 WT were detected by FRNT. $n = 4$–6 mice per group. **c**–**e** Neutralization antibody titre of SARS-CoV-2 BA.5、BQ.1.1 and XBB.1 were detected by FRNT. $n = 4$–6 mice per group. **f** Neutralization titre of SARS-CoV-2 EG.5 and KP.3 were detected by pseudovirus assay. $n = 6$ mice per group. **g** Neutralization titre of SARS-CoV, Pangolin and Ratg13 were detected by pseudovirus assay. **h** Ratio of WT-BQ.1.1 RBD binding IgG2a to IgG1 were determined by ELISA at day 7 and 28 after boost immunisation. $n = 6$ mice per group. Statistical analyses were performed using two-way ANOVA. Data represent two independent experiments. All results are expressed as mean ± SEM. ns, no significantly difference, $^{*}p < 0.05$, $^{**}p < 0.01$, $^{***}p < 0.001$, $^{****}p < 0.0001$.

improve the immunogenicity of RBD-Fc as a mucosal vaccine and to comparing the performance between IN and IM immunisation with the above settings, we would like to investigate the potential of the RBD-Fc vaccine as part of the heterologous immunisation strategy. To this, a group of mice were sequentially immunised with Chadv1 and RBD-Fc through intranasal administration. These novel vaccination strategies were compared with inactivated vaccine and Chadv1, two commonly used COVID-19 vaccines in China which are administered intranasally and intramuscularly respectively. Since a number of previous studies have shown that Fc-fusion proteins were able to elicit significantly stronger humoral responses compared to protein subunits without a Fc fusion[22,34,35], the immunogenicity of the bivalent RBD without a Fc fusion has not been assessed in this study. Control animals were sham-immunised with PBS; as their responses were below the limit of detection (LOD), the level of LOD indicates the level of sham control throughout the rest of the text.

Neutralizing antibody (NAb) titers were similar at day 7 and 28 post-booster for all immunisation groups, except that there was a reduction in titers against the WT strain for the inactivated vaccine and RBD-Fc without CpG adjuvant group, and there was a significant increase for the Chadv1 (IN) + RBD-Fc (IN) group (Supplementary Fig. 2). While inactivated vaccine and Chadv1 elicited comparable levels of response against the WT strain as the RBD-Fc vaccine (Fig. 2b), significantly lower titers were detected against BA.5 (Fig. 2c); and their neutralising activity against BQ.1.1 and XBB.1 diminished (Fig. 2d–e). By contrast, the neutralisation titers induced by RBD-Fc, either through the intramuscular or the intranasal route, or a heterologous regimen of Chadv1+RBD-Fc remained at high

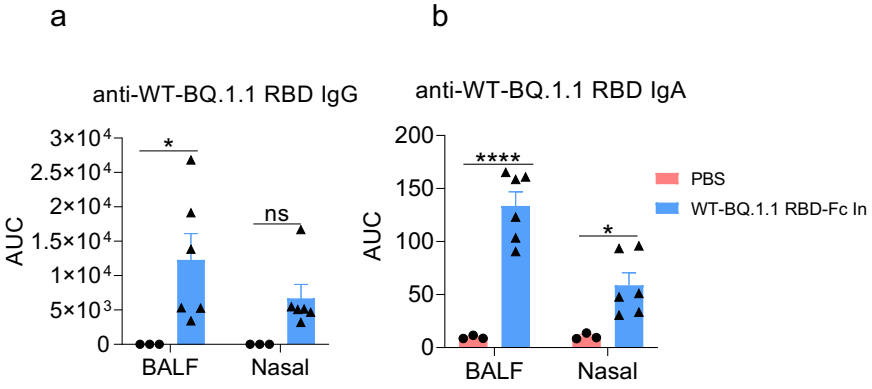

Fig. 3 | Immunisation of WT-BQ.1.1 RBD-Fc induce mucosal immune response in mice. Six-week-old female BALB/c mice were immunised with 10 μg WT-BQ.1.1 RBD-Fc/CpG by intransal. Mice were boosted 4 weeks with homologous antigen dose after primary vaccination. Nasal tissue and BALF were collected at 7 days after the booster immunisation. **a**, **b** Measurement of antigen-specific IgG and IgA antibodies in nasal and BALF by ELISA. Purified WT-BQ.1.1 RBD were the target antigens. The data are shown as the mean ± SEM, $n = 6$ mice per group. Statistical analyses were performed using two-way ANOVA. Data represent two independent experiments. All results are expressed as mean ± SEM. ns, no significantly difference, $^{*}p < 0.05$, $^{**}p < 0.01$, $^{***}p < 0.001$, $^{****}p < 0.0001$.

levels against BA.5, BQ.1.1 and XBB.1 (Fig. 2c–e). For RBD-Fc vaccine, the presence of a CpG adjuvant significantly increased the NAb titers to the level comparable to its intramuscular injection with a SAS adjuvant. Notably, with a pseudovirus neutralisation assay, we showed that the immune sera of RBD-Fc retained neutralising activity against recently emerging SARS-CoV-2 variants including EG.5 and KP.3 (Fig. 2f). In addition, it was able to neutralise SARS-CoV, as well as Pangolin and Pseudotyped Bat Coronavirus Ratg13 which are SARS-like beta-coronaviruses (Fig. 2g).

To assess the Th1/Th2 polarization elicited by the IN immunisation of RBD-Fc vaccine, we measured the ratio of IgG2a to IgG1, since IgG2a is produced through Th1-type cytokines while IgG1 is primarily induced by Th2-type cytokines. It was shown that a mean IgG2a/IgG1 ratio of 0.44 and 0.66 on 7 days and 28 days post-booster, was resulted from IN immunisation of the RBD-Fc vaccine respectively, indicating that Th1-biased responses have been elicited (Fig. 2h).

To examine the durability of antibody responses elicited by the RBD-Fc vaccine, serum samples collected from mice immunised with the inactivated vaccine and those intranasally or intramuscularly immunised with RBD-Fc 3 months after booster was given and used to perform FRNT neutralisation assay. The NAb titers induced by inactivated vaccine dropped significantly towards BA.5 compared to WT and completely diminished for BQ.1.1 and XBB.1. By contrast, RBD-Fc elicited robust NAb responses against all variants, although the titers were lower for BQ.1.1 and XBB.1 (Supplementary Fig. 3a). In general, the neutralisation titers remained largely unchanged for all vaccine group compared to the levels at 7 days post-booster (Supplementary Fig. 3b–e). Therefore, RBD-Fc vaccine is capable of eliciting prolonged antibody responses.

To evaluate the mucosal antibody responses induced by the RBD-Fc vaccine, we measured the IgG and IgA titers against the bivalent WT-BQ.1.1 RBD in Bronchoalveolar-lavage fluid (BALF) and nasal turbinate tissues. Interestingly, while IgG responses in BALF were only marginally different from the sham control and no significant difference found in nasal samples (Fig. 3a), substantial levels of IgA were found in the BALF and significantly higher levels in nasal tissues (Fig. 3b).

RBD-Fc vaccine induced durable protective immunity against viral challenge of XBB.1 in BALB/c mice

Next, we sought to assess the in vivo protective efficacy of RBD-Fc vaccine against SARS-CoV-2. To this end, mice were immunised with a prime-boost regimen at a 28-day interval, homologously with Chadv1 (IN) or RBD-Fc (IN) or heterologously with Chadv1 (IN) + RBD-Fc (IN), followed by intranasal challenge with XBB.1 live virus (Fig. 4a). XBB.1 infection is not lethal to BALB/c mice, so all mice including the sham-immunised ones survived (survival data not shown for simplicity). The changes in weight were monitored throughout a period of 10 days post viral challenge (Fig. 4b). All mice immunised with PBS or Chadv1 exhibited severe body weight loss of up to 10% in the first 2 days but gradually recovered in the next 3 days, followed by another wave of subtle decrease in weight to approximately 95% of the original level after 10 days beyond viral challenge. A similar trend was seen for mice treated with a heterologous prime-boost immunisation of Chadv1 + RBD-Fc, although a much milder initial weight loss of less than 5% was observed. By contrast, no weight loss was seen for mice immunised with the RBD-Fc vaccine. Despite of differences in weight losses observed between groups, lung viral loads were reduced to undetectable levels in all cases, while substantial number of live viruses were detected in sham-immunised mice (Fig. 4c). Accordingly, when lung pathology was examined in the immunised mice, it was found that homologous immunisation of ChAdV1 or the RBD-Fc vaccine, or heterologous immunisation of ChAdV1 and RBD-Fc showed similar patten of mild lymphoid infiltration without severe lung lesions as found in the sham-immunised mice (Fig. 4d).

Since the antibody response against XBB.1 elicited by heterologous immunisation with Chadv1 (IN) + RBD-Fc (IN) was lower than that by homologous immunisation with RBD-Fc (IN) (Fig. 2e), but the severity of lung pathology seemed to be milder when the vaccinated mice were challenged with the virus, we sought to investigate whether this might be attributed to the T cell responses induced by the heterologous immunisation (Fig. 5a). Indeed, in the BALF collected from mice heterologously immunised with Chadv1 (IN) + RBD-Fc (IN), substantial numbers of IFN-γ and TNF secreting $CD4^{+}$ and $CD8^{+}$ T cells were found, with the majority being able to secrete both cytokines (Fig. 5b, c).

To examine the durability of protection offered by the RBD-Fc vaccine, immunised mice were challenged with XBB.1 3 months after booster (Fig. 4e). It was found that the RBD-Fc vaccine was able to keep the mice from detectable viral loads in the lungs, whilst a substantial amount of live virus was found in the lungs of mice immunised with the inactivated vaccine one day after viral challenge although the levels were still significantly lower than the sham immunised group (Fig. 4f). In accordance with this, compared to the sham-immunised mice in which severe lymphoid infiltration with progression to an interstitial pneumonia was found, mice immunised with the inactivated vaccine suffered less severe lung lesions, and the RBD-Fc immunised mice experienced only mild lymphoid infiltrations (Fig. 4g).

Intranasal administration of RBD-Fc vaccine protects K18-hACE2 mice against lethal SARS-CoV-2 challenge

Next, we evaluated the in vivo prophylactic efficacy of the RBD-Fc vaccine against SARS-CoV-2 XBB.1 variant in a lethal K18-hACE2 knock-in mouse model. K18-hACE2 mice were intranasally vaccinated with RBD-Fc with a prime-boost regimen as described above and challenged with a lethal dose of XBB.1 21 days post-boost (Fig. 6a). Although mice immunised with RBD-Fc experienced substantial loss in weight, the reduction was significantly less than the sham-immunised mice did (Fig. 6b). All mice that received placebo administration died by day 5, while the vaccine-immunised group had 100% survival (Fig. 6c). Examination of the post-mortem lungs and brains of infected mice showed that the viral loads from mice immunised with RBD-Fc were below the detection limit (Fig. 6d, e), indicating the clearance of infectious SARS-CoV-2 in these tissues, implying a recovery of body weight

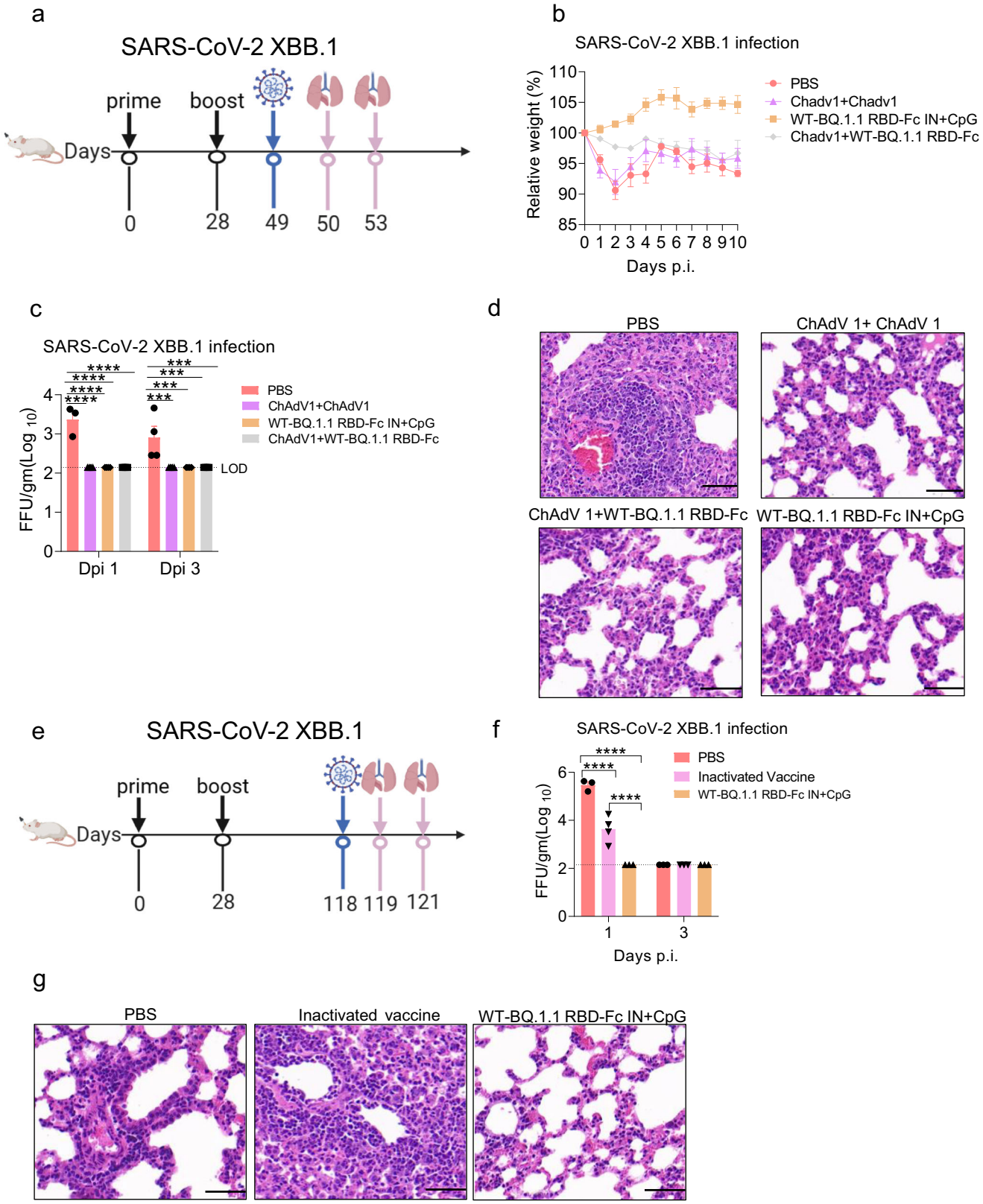

Fig. 4 | WT-BQ.1.1 RBD-Fc immunisation provides protection against SARS-CoV-2 XBB.1 challenge and induce durable immune protection in BALB/c mice. **a** Challenges were conducted at 21 days after the final-immunisation. Mice were intranasally infected with 1×10^5 FFU SARS-CoV-2 KP.3. **b** Weight was monitored daily until day 10 post-infection. **c** Supernatant of homogenates from lung tissues were determined by FFA at day 1 and 3 after infection. Viral load in lung is expressed as FFU/g tissue. $n = 3–4$ mice per group. **d** Sections of paraffin embedded lungs from infected mice were stained with hematoxylin/eosin at day 3 post-infection. Scale bar = 50 μm. **e** Challenges were conducted at 90 days after the final-immunisation. Mice were intranasally infected with 1×10^5 FFU SARS-CoV-2 KP.3. **f** Supernatant of homogenates from lung tissues were determined by a plaque assay at day 1 and 3 after infection. Viral load in lung is expressed as FFU/g tissue. $n = 3–4$ mice per group. **g** Sections of paraffin embedded lungs from infected mice were stained with hematoxylin/eosin at day 3 post-infection. Scale bar = 50 μm. All results are expressed as mean ± SEM. Statistical analyses were performed using two-way ANOVA.

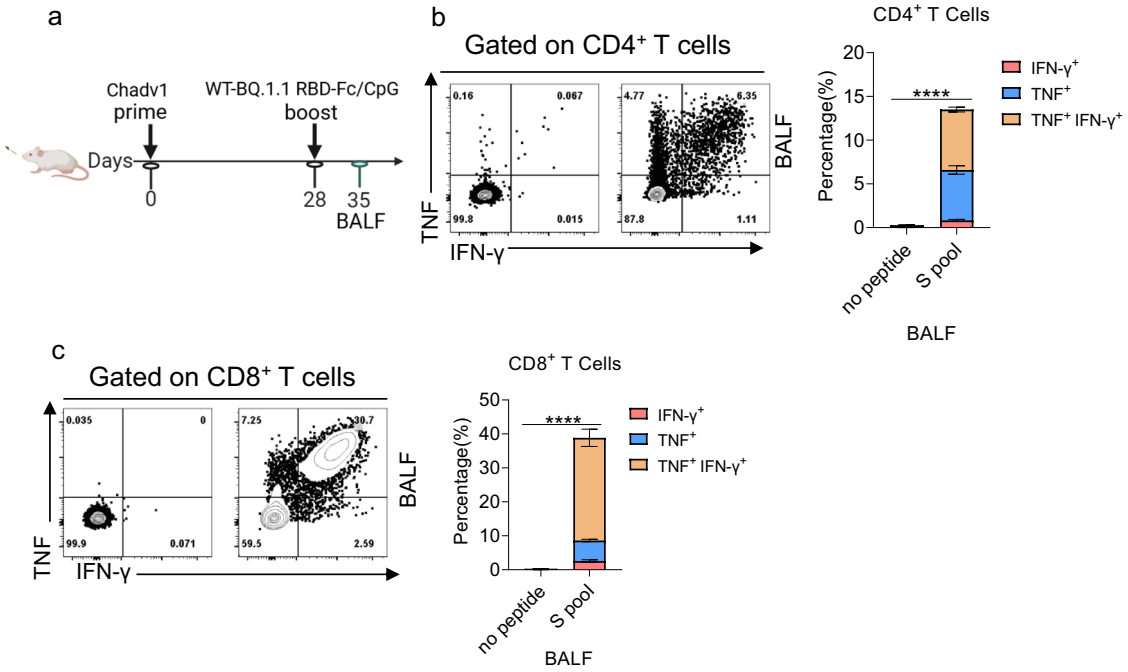

Fig. 5 | Primary immunisation with adenoviral vectored vaccine and boost immunisation with WT-BQ.1.1 RBD-Fc induce durable T cell immune response in BALB/c mice. a 6-week-old female BALB/c mice were administered an adenoviral vectored spike prime by intranasal and boosted with the WT-BQ.1.1 RBD-Fc by intranasal. Bronchoalveolar lavage fluid (BALF) were obtained from the immunised mice at 7 days after the booster immunisation. T cell responses as the percentage of total $CD8^+$ and $CD4^+$ T cells, respectively, were assessed after boosting by intracellular cytokine staining assays in BAL cells. Representative flow plots of Spike-specific $CD4^+$ T cells (**b**, left) and $CD8^+$ T cells (**c**, left). Pooled peptide spike specific IFN-γ^+ TNF^+ $CD4^+$ (**b**, right) and $CD8^+$ T cells (**c**, right). $n = 7–8$ mice per group. Statistical analyses were performed using two-way ANOVA. All results are expressed as mean ± SEM. ns, no significantly difference, $^*p < 0.05$, $^{**}p < 0.01$, $^{***}p < 0.001$, $^{****}p < 0.0001$.

post day 5 as previously observed[32]. By contrast, in the sham-immunised group, whilst the substantial number of viruses in lungs were cleared upon day 4, very high levels of live virus were found in the brains on day 4, explaining the cause of death of these mice (Fig. 6d, e). Importantly, analysis of lung pathology showed that extensive lung lesions and interstitial pneumonia were found in mice of the sham-immunised group, with a large area of fused alveoli walls, edema and haemorrhage; by contrast, only some lymphoid infiltration was found in those immunised with RBD-Fc (Fig. 6f).

Intranasal administration of RBD-Fc vaccine inhibits SARS-CoV-2 infection and transmission in golden hamsters

Golden (Syrian) hamsters have been shown to be a suitable small animal model for the development of vaccines and therapies against SARS-CoV-2, especially concerning the prevention of SARS-CoV-2 transmission[36]. Firstly, we assessed the viral replication of XBB.1 in the respiratory tract of golden hamsters to judge if the RBD-Fc vaccine can control the infection of XBB.1 in these animals. 6–8 weeks-old female golden hamsters received intranasal or intramuscular administration of 10 μg RBD-Fc or placebo, followed by a first boost 28 days post priming and a second boost 28 days thereafter. All hamsters were intranasally challenged with 1×10^5 PFU of SARS-CoV-2 XBB.1 strain 14 days after the second boot. Three days after viral challenge, lung and nasal turbinate tissues were collected for determination of viral loads using a plaqueformation assay (Fig. 7a). It was shown that XBB.1 replicated to high virus titres in lung tissues and nasal tissues in sham-immunised hamsters. Both intranasal and intramuscular vaccination of RBD-Fc significantly reduced the viral loads in lungs. By contrast, only intranasal vaccination of RBD-Fc was able to result in significant decrease in virus titres in the nasal tissues; although a decrease was seen following intramuscular vaccination this was not statistically significant (Fig. 7b).

Next, we explored whether the RBD-Fc vaccine could be effective in limiting host-host transmission. To this, the close contact transmission model with golden hamsters was chosen as has been shown to be a more efficient way of ensuring transmission compared to the non-contact transmission model[36]. Accordingly, hamsters were firstly intranasally challenged with 1×10^5 PFU of XBB.1 immunised intranasally or intramuscularly with RBD-Fc or placebo as described above. 24 h later, the SARS-CoV-2–challenged donor hamsters were co-housed with naïve hamsters immunised with RBD-Fc (IM or IN) or PBS control for 24 h in a 1:1 ratio. Two days later, the contact hamsters were sacrificed for examination of virus titers in lung and nasal turbinate tissues (Fig. 7c). Despite using this aggressive contact transmission model, the viral loads detected in the lungs of hamsters received placebo were much lower than the donor, and no significant difference in lung viral titers was found between the sham-immunised hamsters and vaccinated hamsters. Nevertheless, the virus titers in the nasal turbinate tissues of sham-immunised hamsters were comparable to the levels found in the donors, and a significant reduction in the amount of live virus was found between the sham-immunised hamsters and those intranasally immunised with the RBD-Fc vaccine (Fig. 7d).

Discussion

Although COVID-19 is no longer an international public health emergency, SARS-CoV-2 continues to circulate globally. Despite being less deadly compared to the ancestral strain and the early beta and delta variants, it continues to evolve to gain capacity for immune evasion and transmission, resulting in sickness of varying degrees and even death. To overcome viral immune evasion, manufacturers have been updating the vaccine components by using the latest dominant strain. However, currently COVID-19 vaccines are given largely through intramuscular injections which has been shown to induce mainly systemic immunity and only weak respiratory mucosal immunity[37]. Thus substantial mucosal humoral and cellular immunity are induced in convalescent individuals while such mucosal responses are very limited or absent in vaccinated individuals without a SARS-CoV-2 infection history, indicating the importance of vaccination at the site of infection[37–39]. Thus it is becoming accepted that mucosal

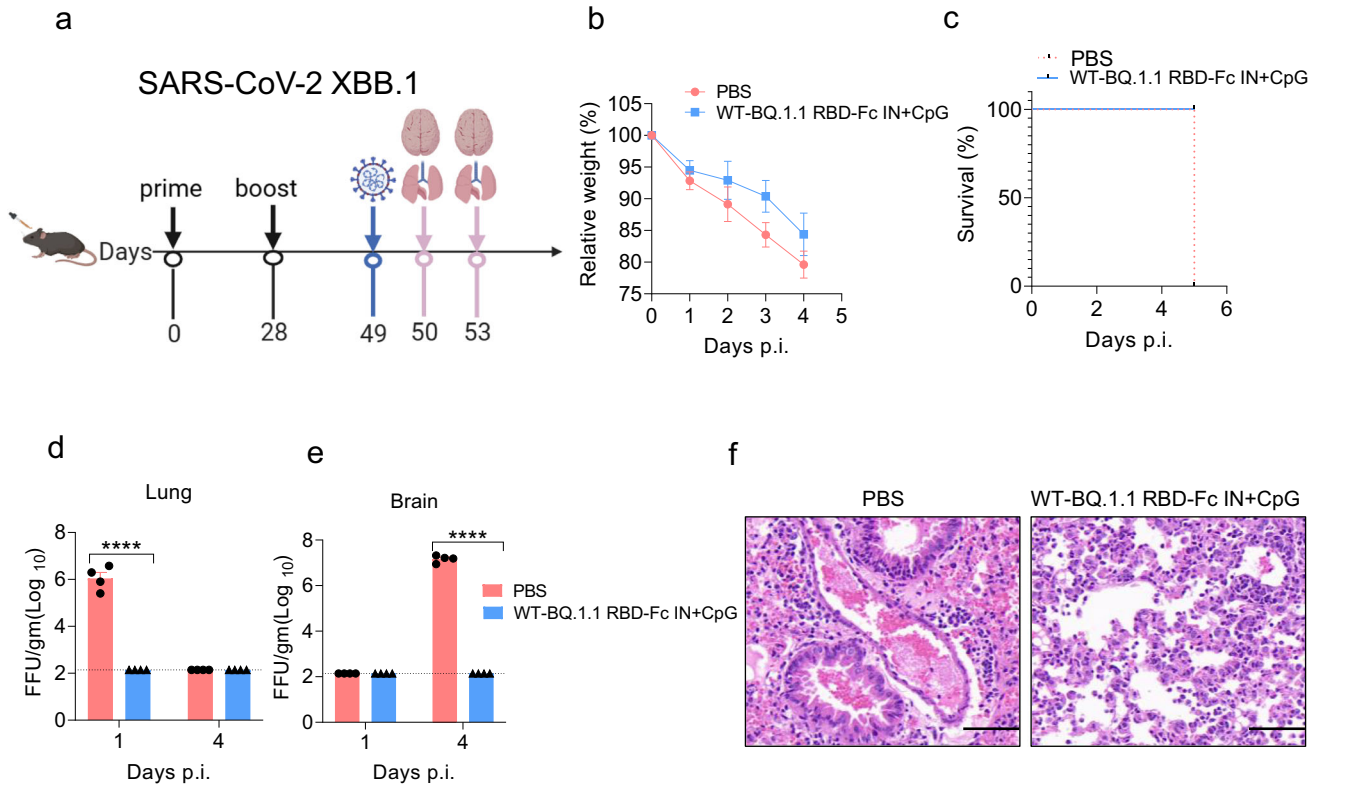

Fig. 6 | WT-BQ.1.1 RBD-Fc immunisation provides protection against SARS-CoV-2 XBB.1 challenge in K18-hACE2 mice. a Challenges were conducted at 21 days after the final-immunisation. Mice were intranasally infected with 1×10^5 FFU SARS-CoV-2 KP.3. **b**, **c** Weight and mortality were monitored daily until day 4 post-infection. Mice were all dead in the PBS group at day 5 post-infection. **d**, **e** Supernatant of homogenates from lung and brain tissues were determined by FFA at day 1 and 3 after infection. Viral load in lung and brain is expressed as FFU/g tissue. $n = 4$ mice per group. **f** Sections of paraffin embedded lungs from infected mice were stained with hematoxylin/eosin at day 3 post-infection. Scale bar = 50 μm. All results are expressed as mean ± SEM. Statistical analyses were performed using two-way ANOVA.

immunity may be required to block infection and onward transmission. However, clinical data from mucosal COVID-19 vaccines in humans is very limited, and recent trails of intranasal vaccination of an adenovirus-vectored COVID-19 vaccines failed to induce consistent and robust mucosal responses[40]. The route of immunisation may be crucial, as it was shown that intratracheal boosting with a bivalent Ad26-based SARS-CoV-2 vaccine was superior to intramuscular or intranasal administration of the same vaccine in eliciting robust mucosal immunity in macaques[41]. An optimised way for delivery could therefore enhance the efficacy of mucosal vaccines such as the RBD-Fc vaccine as investigated here.

In addition to adenovirus-vectored vaccines, Fc-fusion proteins can be used as mucosal vaccines, as the Fc fragment can cross the airway mucosal barrier in a FcRn-dependent manner. Since the SARS-CoV-2 spike RBD is highly immunogenic and an ideal immunogen to be presented by the Fc fragment, we constructed a bivalent RBD-Fc vaccine by fusion of tandem RBDs from the ancestral and BQ.1.1 strain to an engineered human IgG4 Fc fragment. By labelling RBD-Fc with a far-red fluorescent dye, we evaluated the biodistribution of the vaccine through *ex vivo* imaging in mice. RBD-Fc was able to more efficiently reach the lungs of mice and attain better retention in both nasal cavity and lungs compared to a bivalent RBD without Fc (Fig. 1).

We also performed immunogenicity and virus challenge studies of the RBD-Fc vaccine and demonstrated that it was able to elicit robust humoral immune responses through a prime-boost immunisation regimen, via either intramuscular or intranasal delivery (Figs. 2, 3). The vaccine serum showed strong and durable neutralisation activity against recent SARS-CoV-2 variants including XBB.1 which has escaped inactivated or adenovirus-vectored vaccines containing only the ancestral strain immunogen. Mice intranasally immunised with the RBD-Fc vaccine were effectively protected from viral challenge of SARS-CoV-2 XBB.1, in not only the BALB/c mouse (Fig. 4) model but also the lethal K18-hACE2 knock-in mouse model (Fig. 6), with the lung and nasal viral loads reduced to undetectable levels and limited pathological changes in lungs. As the RBD-Fc vaccine only bears a weak CD4 T cell epitope (S444-458) according to a previous publication by Zhuang et al.[42], protection is presumably to be largely offered by the potently elicited neutralisation antibody responses. In a golden hamster model, intranasal immunisation of the RBD-Fc vaccine was able to more effectively limit viral transmission through direct contact compared to intramuscular immunisation (Fig. 7), which is probably attributed to the IgA responses elicited by the mucosal vaccine (Fig. 3).

Previous studies of immunisation with SARS-CoV-2 vaccines through the mucosal routes have largely focused on the use of intranasal administration[43–45]. However, a clinical trial showed that the mucosal and systemic immune responses induced by intranasal administration of an adenovirus-vectored COVID-19 vaccine ChAdOx1 nCoV-19 (AZD1222, University of Oxford / AstraZeneca) were relatively weak and inconsistent[40]. Recently, McMahan and colleagues compared the immune responses elicited by boosting of an Ad26 adenoviral vector-based vaccine of SARS-CoV-2 in rhesus macaques through intranasal and intratracheal route[41]. Strikingly, substantially greater levels of NAb titers, IgA spike-specific binding antibody responses and T-cell responses were found in the nasal swab and BALF in the intratracheal group compared to the intranasal group. In accordance with this, markedly lower levels of viral loads were found in the nasal swab and BALF in the intratracheal group and provided near-complete protection against high-dose SARS-CoV-2 BQ.1.1 challenge. This study highlighted the importance of a suitable means for administration of mucosal vaccines to maximise their efficacies. Here, while we have demonstrated the feasibility of delivering the RBD-Fc vaccine through the intranasal route, it is expected that delivery of the vaccine through the

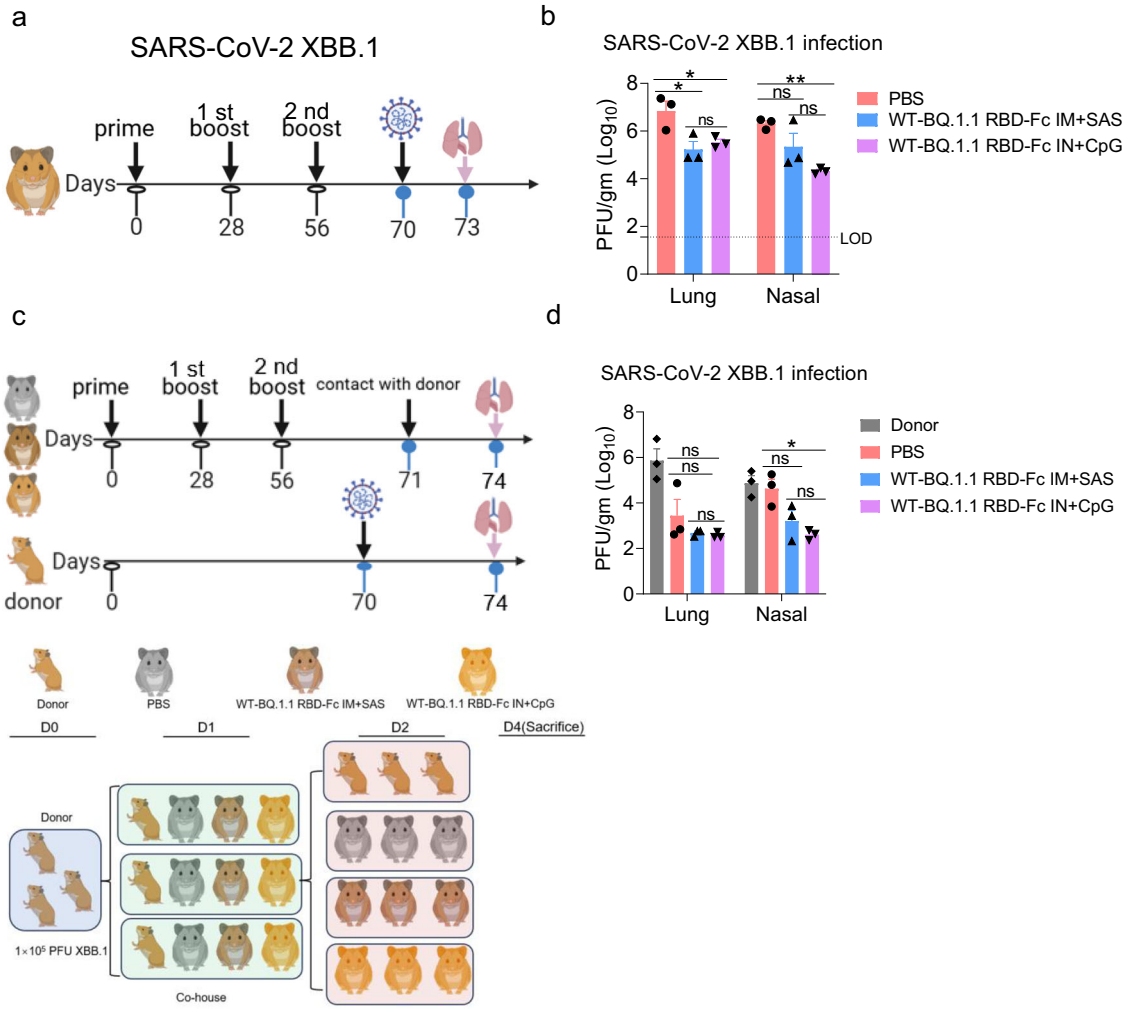

Fig. 7 | WT-BQ.1.1 RBD-Fc immunisation provides protection against SARS-CoV-2 XBB.1 challenge and transmit in hamster. a Challenges were conducted at 14 days after the final-immunisation. Hamster were intranasally infected with 1×10^5 FFU SARS-CoV-2 KP.3. **b** Supernatant of homogenates from lung and nasal tissues were determined by the plaque assay at day 3 after infection. Viral load in lung and nasal is expressed as PFU/g tissue. $n = 3$ hamsters per group. **c** Hamsters were immunised with PBS, WT-BQ.1.1 RBD-Fc/ CpG by in and WT-BQ.1.1 RBD-Fc / SAS by im. 14 days after the final immunisation, each of immunised hamster was transferred to a new cage and were cohoused with one donor hamster in a one-to-one manner. The donor hamsters ($n = 4$) were infected with 1×10^5 PFU of SARS-CoV-2 XBB.1 through the intranasal route at 24 h prior to cohouse. **d** Supernatant of homogenates from lung and nasal tissues were determined by the plaque assay at day 2 after cohouse. All results are expressed as mean ± SEM. Statistical analyses were performed using two-way ANOVA.

intratracheal route or a suitable nebulizer device could further enhance the immune responses elicited by the vaccine and improve the protection provided.

One interesting observation in this study was that the neutralisation titers elicited by heterologous immunisation of Chadv1 (an adenoviral vector-based vaccine of the ancestral strain) and the bivalent RBD-Fc vaccine (encoding both ancestral and BQ.1.1 RBDs) was comparable to homologous immunisation of the RBD-Fc vaccine against the pre-Omicron ancestral strain (Fig. 2b), but substantially lower against BA.5, BQ.1.1 and XBB.1 (Fig. 2c–e). In contrast there emerging evidence that the heterologous boosting strategy is superior to homologous boosting[46–48]. However, the reposted studies are based on the vaccination of antigen derived from the ancestral strain, and when immunogens from different strains are involved, the impact of the so-called 'immune imprinting' might dominate over the benefit resulted from heterologous immunisation. That said, for individuals that have been immunologically exposed to the ancestral spike component of SARS-CoV-2 through either vaccination or infection or both, further vaccination of the SARS-CoV-2 spike containing an ancestral strain component may skew the induced antibody responses towards the established 'antibody sink' and away from variant-specific antibody responses. Therefore, for individuals pre-exposed to the spike of an ancestral strain, it may be beneficial to receive a single-component variant-specific vaccine. As a consequence, FDA has now advised manufacturers that the COVID-19 vaccines (2024–2025 formula) should be monovalent JN.1/KP.2 vaccines (fda.gov). On the other hand, for individuals without pre-exposure, a bivalent vaccine containing the ancestral strain and latest variant may offer more protection, as the two genetically and antigenically distant strains can elicit cross-reactivity against the conserved epitopes without compromising the variant-specific antibody responses.

Nonetheless, although heterologous immunisation with Chadv1 (IN) + RBD-Fc (IN) elicited lower NAb titers against XBB.1 compared to homologous immunisation with RBD-Fc (Fig. 2e), we found that heterologous immunisation seemed to result in a better lung pathology profile with apparently milder lymphoid infiltration (Fig. 4d). We found that including a single shot of Chadv1 (IN) as priming was sufficient to elicit the strong virus-specific T cell responses shown to be vital to viral control[49], which are absent in RBD vaccines due to lack of potent T cell epitopes. Therefore, heterologous immunisation with a spike-based adenoviral vectored vaccine and an RBD-Fc vaccine with the appropriate strains included could be an ideal COVID-19 vaccination strategy.

In summary, using the recombinant Fc-fusion vaccine technology, we prepared a bivalent RBD-Fc vaccine that incorporates the RBDs from ancestral and BQ.1.1 strains. To our knowledge, this is one of the few studies demonstrating the visual evidence that an RBD-Fc vaccine can be used as a mucosal vaccine and effectively delivered to the lungs, eliciting robust and durable humoral responses, conferring significant protection against SARS-CoV-2 challenge in mouse models. Importantly, it is more effective in limiting viral infection through intranasal over intramuscular administration in a golden hamster transmission model. These promising preclinical results validate the potential benefits of this Fc-fusion vaccine technology for the control of respiratory infections, especially as a heterologous immunisation option.

Methods

Ethics statement

The handling of mice and experimental procedures were approved by the Animal Welfare and Research Ethics Committee of the First Affiliated Hospital of Guangzhou Medical University (2022025). The hamster studies and experimental procedures were approved by the Ethics Committee of the Wuhan Institute of Virology, Chinese Academy of Sciences. The mice challenge experiments were conducted under animal biosafety level 3 (ABSL3) facility in Guangzhou Customs District Technology Center, which were approved by the Ethics Committee of the Guangzhou Customs District Technology Center. Hamster challenge studies were conducted under animal biosafety level 3 (ABSL3) facility in the Wuhan Institute of Virology, Chinese Academy of Sciences, which were approved by the Ethics Committee of the Wuhan Institute of Virology, Chinese Academy of Sciences.

Cell lines and virus

Vero E6 cells, 293 T- human ACE2 cells were maintained in high glucose Dulbecco's Modified Eagle Medium (DMEM, Gibco) supplemented with L-glutamine, sodium pyruvate, and 10% fetal bovine serum (FBS). These cells were cultured at 37 °C and 5% CO_2 in a humidified atmosphere. Freestyle 293 F cell lines were maintained in Freestyle 293 expression medium, and cultured at 37 °C and 8% CO_2 with 120 rpm in a humidified atmosphere. The SARS-CoV-2 variants, including WT, BA.5, BQ.1.1, XBB.1 were isolated from COVID-19 patients and preserved in Guangzhou Customs District Technology Center BSL-3 Laboratory. Experiments related to authentic SARS-CoV-2 were conducted in Guangzhou Customs District Technology Center BSL-3 Laboratory.

Expression constructs

All genes used in this study were synthesized by GenScript and codon optimized for human host. To avoid autoimmune reactions, the sequence of IgG4 Fc used in our study was constructed as previous reported. Briefly, to construct the WT-BQ.1.1 RBD-Fc, the RBD sequence (WT RBD: PDB #7XSC_E; BQ.1.1 RBD: PDB # 8IF2_B) were fused to the 3′ end of the IgG4 Fc with a $(SG3)_2$ linker. WT RBD and BQ.1.1 RBD were linked with a nine residue Gly-Ser linker. To obtain the secreted protein, an IL-2 signal sequence was attached upstream of the RBD.

Biosynthesis of recombinant proteins and purification

The expression vectors were transiently transfected into Freestyle 293 F cell lines using the PEI transfection reagents. 7 days after transfection, the supernatants were collected and centrifuged to remove the cell ribs. The WT-BQ.1.1 RBD-Fc and WT-BQ.1.1 RBD were purified by the affinity chromatography using NTA-His at pH 7.4 (Cytiva).

Size exclusion chromatography

Gel filtration was performed on the Cytiva ÄKTA-Purifier system using a Superdex 200 Increase 10/300 GL(GE) column. The column was equilibrated with 100 ml 0.01 M phosphate buffer, 0.14 M NaCl, pH 7.4. Elution of proteins (WT-BQ.1.1 RBD-Fc and WT-BQ.1.1 RBD) were detected by recording the absorption at 280 nm with a flow rate of 0.5 ml/min at room temperature.

Biodistribution of WT-BQ.1.1 RBD-Fc in mice

To track the biodistribution of WT-BQ.1.1 RBD-Fc in mice after inhalation, fluorescent dye Cy5 was loaded into WT-BQ.1.1 RBD-Fc and WT-BQ.1.1 RBD. Briefly, a 10-fold molar excess of Cy5 reagent to label 1–10 mg/mL WT-BQ.1.1 RBD-Fc and WT-BQ.1.1 RBD. Incubate reaction in dark for two hours at room temperature and shacked with 120 rpm. Then remove excess Cy5 reagent using a desalting column. 6 weeks old female BALB/c mice were instilled with 15.6 μg WT-BQ.1.1 RBD-Fc or 10 μg WT-BQ.1.1 RBD in a 50 μl volume. Mice were sacrificed at 4 h, 24 h, 48 h and 72 h post-instilled. The collected nose and lungs were imaged by a Live Imager.

Enzyme-linked immunosorbent assay (ELISA)

The 96- well plates were coated with 1 μg/ml SARS-CoV-2 WT-BQ.1.1 RBD produced in-house, and incubated overnight at 4 °C. Wells were washed for three times and blocked for 1 hr at 37 °C. A series two-fold dilution of BALF supernatant and nasal homogenate (starting at 1:50) were added and incubated for 2 hr at 37 °C. Bound antibodies were detected with horseradish peroxidase (HRP)- labeled goat anti- mouse IgA secondary antibody (Protech, 1:1000) at 37 °C for 1 hr. Binding signals were visualized using a TMB substrate and the reaction was stopped by adding 2 M H_2SO_4. The light absorbance at 450 nm was measured by a microplate reader (Bioteck).

Preparation of cells from BALF

Mice were euthanized by excessive anesthetized with intraperitoneal tribromoethanol at the indicated time points. BALF was acquired by inflating lungs with 1 ml complete RPMI 1640 medium via cannulation of the trachea followed by lavaging three times. Cells in the BALF were collected by centrifugation at 300 g 5 min to remove the supernatant.

Flow cytometry

For Intracellular cytokine staining (ICS), lymphocytes were cultured in 96-well plates at 37 °C for 5–6 h in the presence of SARS-CoV-2 WT spike peptides pool and brefeldin A (BD Biosciences). Cells were then labelled for cell surface markers: anti-mouse CD8α-Alexa 488 (clone 53–6.7; 100723; Biolegend), anti-mouse CD16/32-PerCP-Cy5.5 (clone 93; 45–0161-82; eBioscience), anti-mouse CD4-Brilliant Violet 510 (clone GK1.5; 100449; Biolegend) at 4 °C for 15 min in the dark, fixed/permeabilized with Cytofix/Cytoperm Solution (BD Biosciences), and labelled with intracellular antibody cocktails, included anti-mouse TNF-PE (clone MP6-XT22; 12–7321-82; eBioscience) and anti-mouse IFN-γ-APC (clone XMG1.2; 17–7311-82; eBioscience). All flow cytometry data were acquired on a BD FACS Verse Cytometer and were analyzed using FlowJo software.

Focus formation assay (FFA)

1.8×10^4 /well Vero E6 cells were seed into 96-well plate. 16 h later, virus serum mixture or lung homogenate were serially diluted and incubated at 37 °C for 24 h with 5% CO_2. 24 h later, plates were fixed with 4% paraformaldehyde for 30 min and permeabilized with 0.2% Triton X-100. Cells were then stained with rabbit anti-SARS-CoV-2 N protein polyclonal antibody at 37 °C for 2 h. Plates were washed with PBST three times, and followed by an HRP-labeled goat anti-rabbit secondary antibody (Cat. No.: 109-035-088, Jackson ImmunoResearch Laboratories, Inc. West Grove, PA). The foci were visualized by TrueBlue Peroxidase Substrate (KPL, Gaithersburg, MD), and counted with an ELISPOT reader (Cellular Technology Ltd. Cleveland, OH).

Live SARS-CoV-2 neutralization assay

The live virus neutralization assay was conducted in a BSL-3 facility. Briefly, serum from immunised mice were inactivated at 56 °C for 30 min to eliminate the effect of complement. Then the serum was 4-fold serially diluted and mixed with the same volume of SARS-CoV-2 WT, BA.5, BQ.1.1, XBB.1 (200 FFU/well), incubated at 37 °C for 1 h. Then the mixture was abandoned and add 100 μl 1.6% CMC each well. The plates were incubated in a CO_2 incubator at 37 °C for 24 h. 24 h later, plates were fixed and FFA was used to detect the neutralization titres.

Pseudovirus neutralization assay

Plasmids of pcDNA3.1 carrying SARS-CoV-2 EG.5, KP.3 and SARS-CoV, Pangolin, Ratg13, spike genes were used for generating pseudoviral particles together with the lentiviral packaging vector and transfer vector encoding luciferase reporter. All the constructs were sequence confirmed. The pseudoviral neutralization test has been described previously. Briefly, the neutralizing activity of serum from immunised mice were inactivated at 56 °C for 30 min to eliminate the effect of complement. Four-fold serial diluted serum were incubated with pseudoviral particles at 37 °C, 5% CO_2 for 1 h. Stable HEK293T cells expressing human ACE2 were then added to the mixture at 3×10^4 cells/well. 48 h post infection, culture supernatants were removed and 50 μl of Bright-Glo Luciferase assay system (Promega, USA) was added to each well. The reaction was incubated at room temperature for 5 min and firefly luciferase activity was measured. The percentage neutralization was calculated relative to the control.

Immunisation and infection of mice

Mice homologous immunisation: 6–8 weeks-old female BALB/c mice were immunised with 10 μg WT-BQ.1.1 RBD-Fc with SAS adjuvant by intramuscular route. Three weeks later, boost immunisation with the same dose; 6–8 weeks-old female BALB/c mice were immunised with 10 μg WT-BQ.1.1 RBD-Fc alone or with CpG adjuvant by intranasal route. Three weeks later, boost immunisation with the same dose; 6–8 weeks-old female BALB/c mice were immunised with 50 μl inactivated vaccine (SINOVAC) by intramuscular route. Three weeks later, boost immunisation with the same dose; 6–8 weeks-old female BALB/c mice were immunised intranasally with 3.8×10^8 viral particle of Ad5-nCoV (Convidecia). Three weeks later, boost immunisation with the same dose. Mice heterologous immunisation: 6-8 weeks-old female BALB/c mice were lightly anesthetized with isoflurane and then immunised intranasally with 3.8×10^8 viral particle of Ad5-nCoV (Convidecia). Three weeks later, boost immunisation with the 10 μg WT-BQ.1.1 RBD-Fc with CpG adjuvant by intranasal route. SARS-CoV-2 challenge experiments: Three weeks or three months later after the final immunisation, mice were lightly anesthetized with isoflurane and then directly infected with 1×10^5 FFU SARS-CoV-2 XBB.1 virus in a total volume of 50 μl via intranasal administration.

Immunisation and infection of hamsters

8–10 weeks-old female golden hamster were immunised with 30 μg WT-BQ.1.1 RBD-Fc with CpG adjuvant by intranasal route or 30 μg WT-BQ.1.1 RBD-Fc with SAS adjuvant by intramuscular route. Four weeks later, hamsters were booster with the same antigen dose. Eight weeks later, hamsters were again booster with the same antigen dose. Four weeks after the final immunisation, hamsters were lightly anesthetized with isoflurane and directly infected with 1×10^5 FFU SARS-CoV-2 XBB.1 virus in a total volume of 50 μl per mouse via intranasal administration. In the contact transmission model, hamsters were kept in Biosafety Level-2 housing. The viral challenge experiments were then conducted in Biosafety Level-3 animal facility following SOPs strictly. 8 weeks-old female hamsters were used for in vivo evaluation of WT-BQ.1.1 RBD-Fc intranasal immunisation in preventing contact transmission of SARS-CoV-2. 3 donor hamsters were intranasally infected with 1×10^5 PFU of SARS-CoV-2 XBB.1 at 0 dpi. At 24 dpi, each donor hamster was co-housed with three immunised hamsters (PBS immunised, WT-BQ.1.1 RBD-Fc/SAS intramuscular immunised and WT-BQ.1.1 RBD-Fc/CpG intranasal immunised) for 24 h as a close contact. After co-housing, hamsters were then separated and housed in a new single cage. All the hamsters were sacrificed at day 2 after co-housing. Nasal turbinate and lung tissues were collected for viral load determination by plaque assay.

Detection of viral load in lungs

Mice were euthanized by excessive anesthetized with intraperitoneal tribromoethanol. Removed the lung tissue after mice were sacrificed. Lung tissue were homogenized in 1 mL of DPBS medium, and then frozen at −80 °C. After freezing and thawing, lung homogenate was clarified by centrifugation at 5000 g for 10 min at 4 °C. Viral titres in supernatant were determined by Vero E6 cell lines. Briefly, 1.8×10^4 /well cells were seeded on the 96-well plates. Then, 50 μl of 10-fold serially diluted suspension was added to each well, and then incubation at 37 °C for 1 h. Discard the supernatant, add 100 μl 1.6% CMC in each well. The plates were incubated in a CO_2 incubator at 37 °C for 24 h, and then the plates were fixed with 4% paraformaldehyde for 30 min. Then the plates were determined as the FFA according to the previous described.

Statistical analysis

Data are represented in scatter dot plots. Statistical analysis was done by 2-Way ANOVA (with Geisser-Greenhouse correction) for comparisons within vaccines of immunisation (Fig. 2). Differences between two groups were analyzed by 2-Way ANOVA (Fig. 3). Two-way ANOVA followed by multiple comparisons was used to compare pairs of groups (Figs. 4, 5, 6). GraphPad Prism 9.0 was used for statistical analysis and plotting the graphs.

Data availability

Sequences data that support the findings of this study have been downloaded from the Protein Data Bank with the primary accession code WT RBD: PDB #7XSC_E; BQ.1.1 RBD: PDB # 8IF2_B.

Received: 8 February 2025; Accepted: 7 May 2025;
Published online: 18 May 2025

References

1. Watson, O. J. et al. Global impact of the first year of COVID-19 vaccination: a mathematical modelling study. *Lancet Infect. Dis.* **22**, 1293–1302 (2022).
2. Altmann, D. M. & Boyton, R. J. COVID-19 vaccination: The road ahead. *Science* **375**, 1127–1132 (2022).
3. Eyre, D. W. et al. Effect of COVID-19 Vaccination on Transmission of Alpha and Delta Variants. *N. Engl. J. Med* **386**, 744–756 (2022).
4. Lau, J. J. et al. Real-world COVID-19 vaccine effectiveness against the Omicron BA.2 variant in a SARS-CoV-2 infection-naive population. *Nat. Med* **29**, 348–357 (2023).
5. Dejnirattisai, W. et al. SARS-CoV-2 Omicron-B.1.1.529 leads to widespread escape from neutralizing antibody responses. *Cell* **185**, 467–484.e415 (2022).
6. Wang, Q. et al. Alarming antibody evasion properties of rising SARS-CoV-2 BQ and XBB subvariants. *Cell* **186**, 279–286 e278 (2023).
7. Yang, S. et al. Fast evolution of SARS-CoV-2 BA.2.86 to JN.1 under heavy immune pressure. *Lancet Infect. Dis.* **24**, e70–e72 (2024).
8. Zhu, A. et al. Antigenic characterization of SARS-CoV-2 Omicron subvariants XBB.1.5, BQ.1, BQ.1.1, BF.7 and BA.2.75.2. *Signal Transduct. Target. Ther.* **8**, 125 (2023).
9. Cao, Y. et al. Imprinted SARS-CoV-2 humoral immunity induces convergent Omicron RBD evolution. *Nature* **614**, 521–529 (2023).
10. Miller, J. et al. Substantial Neutralization Escape by SARS-CoV-2 Omicron Variants BQ.1.1 and XBB.1. *N. Engl. J. Med* **388**, 662–664 (2023).
11. Levy, M. E. et al. Reduced Likelihood of Hospitalization With the JN.1 or HV.1 Severe Acute Respiratory Syndrome Coronavirus 2 Variants Compared With the EG.5 Variant. *J. Infect. Dis.* **230**, 1197–1201 (2024).
12. Xie, Y., Choi, T. & Al-Aly, Z. Mortality in Patients Hospitalized for COVID-19 vs Influenza in Fall-Winter 2023-2024. *JAMA* **331**, 1963–1965 (2024).
13. Davis, H. E., McCorkell, L., Vogel, J. M. & Topol, E. J. Long COVID: major findings, mechanisms and recommendations. *Nat. Rev. Microbiol* **21**, 133–146 (2023).
14. Israel, A. et al. Elapsed time since BNT162b2 vaccine and risk of SARS-CoV-2 infection: test negative design study. *BMJ* **375**, e067873 (2021).
15. Levin, E. G. et al. Waning Immune Humoral Response to BNT162b2 Covid-19 Vaccine over 6 Months. *N. Engl. J. Med* **385**, e84 (2021).

16. Azzi, L. et al. Mucosal immune response in BNT162b2 COVID-19 vaccine recipients. *EBioMedicine* **75**, 103788 (2022).
17. Aksyuk, A. A. et al. AZD1222-induced nasal antibody responses are shaped by prior SARS-CoV-2 infection and correlate with virologic outcomes in breakthrough infection. *Cell Rep. Med* **4**, 100882 (2023).
18. Froberg, J. & Diavatopoulos, D. A. Mucosal immunity to severe acute respiratory syndrome coronavirus 2 infection. *Curr. Opin. Infect. Dis.* **34**, 181–186 (2021).
19. Procter, T. D. et al. Thrombosis with thrombocytopenia syndrome (TTS) following adenovirus vector COVID-19 vaccination in Canada. *Vaccine* **41**, 6802–6809 (2023).
20. Alu, A. et al. Intranasal COVID-19 vaccines: From bench to bed. *EBioMedicine* **76**, 103841 (2022).
21. Fieux, M. et al. FcRn as a Transporter for Nasal Delivery of Biologics: A Systematic Review. *Int J Mol Sci* **22** https://doi.org/10.3390/ijms22126475 (2021).
22. Ye, L., Zeng, R., Bai, Y., Roopenian, D. C. & Zhu, X. Efficient mucosal vaccination mediated by the neonatal Fc receptor. *Nat. Biotechnol.* **29**, 158–163 (2011).
23. Slifka, M. K. & Amanna, I. J. Role of Multivalency and Antigenic Threshold in Generating Protective Antibody Responses. *Front Immunol.* **10**, 956 (2019).
24. Lan, J. et al. Structure of the SARS-CoV-2 spike receptor-binding domain bound to the ACE2 receptor. *Nature* **581**, 215–220 (2020).
25. Dejnirattisai, W. et al. The antigenic anatomy of SARS-CoV-2 receptor binding domain. *Cell* **184**, 2183–2200.e2122 (2021).
26. Yuan, M. et al. Structural basis of a shared antibody response to SARS-CoV-2. *Science* **369**, 1119–1123 (2020).
27. Barnes, C. O. et al. SARS-CoV-2 neutralizing antibody structures inform therapeutic strategies. *Nature* **588**, 682–687 (2020).
28. Nutalai, R. et al. Potent cross-reactive antibodies following Omicron breakthrough in vaccinees. *Cell* **185**, 2116–2131.e2118 (2022).
29. Huo, J. et al. Neutralization of SARS-CoV-2 by Destruction of the Prefusion Spike. *Cell Host Microbe* **28**, 497 (2020).
30. Zhou, D. et al. Structural basis for the neutralization of SARS-CoV-2 by an antibody from a convalescent patient. *Nat. Struct. Mol. Biol.* **27**, 950–958 (2020).
31. Wang, Q. et al. XBB.1.5 monovalent mRNA vaccine booster elicits robust neutralizing antibodies against XBB subvariants and JN.1. *Cell Host Microbe* **32**, 315–321.e313 (2024).
32. Zhang, Y. et al. Mosaic RBD Nanoparticles Elicit Protective Immunity Against Multiple Human Coronaviruses in Animal Models. *Adv. Sci. (Weinh.)* **11**, e2303366 (2024).
33. Pesce, I. et al. Intranasal administration of CpG induces a rapid and transient cytokine response followed by dendritic and natural killer cell activation and recruitment in the mouse lung. *J. Innate Immun.* **2**, 144–159 (2010).
34. Ochsner, S. P. et al. FcRn-Targeted Mucosal Vaccination against Influenza Virus Infection. *J. Immunol.* **207**, 1310–1321 (2021).
35. Zhang, Y. et al. A novel RSV F-Fc fusion protein vaccine reduces lung injury induced by respiratory syncytial virus infection. *Antivir. Res* **165**, 11–22 (2019).
36. Sia, S. F. et al. Pathogenesis and transmission of SARS-CoV-2 in golden hamsters. *Nature* **583**, 834–838 (2020).
37. Tang, J. et al. Respiratory mucosal immunity against SARS-CoV-2 after mRNA vaccination. *Sci. Immunol.* **7**, eadd4853 (2022).
38. Puhach, O. et al. SARS-CoV-2 convalescence and hybrid immunity elicits mucosal immune responses. *EBioMedicine* **98**, 104893 (2023).
39. Poon, M. M. L. et al. SARS-CoV-2 infection generates tissue-localized immunological memory in humans. *Sci. Immunol.* **6**, eabl9105 (2021).
40. Madhavan, M. et al. Tolerability and immunogenicity of an intranasally-administered adenovirus-vectored COVID-19 vaccine: An open-label partially-randomised ascending dose phase I trial. *EBioMedicine* **85**, 104298 (2022).
41. McMahan, K. et al. Mucosal boosting enhances vaccine protection against SARS-CoV-2 in macaques. *Nature* **626**, 385–391 (2024).
42. Zhuang, Z. et al. Mapping and role of T cell response in SARS-CoV-2-infected mice. *J. Exp. Med.* **218**, https://doi.org/10.1084/jem.20202187 (2021).
43. Feng, L. et al. An adenovirus-vectored COVID-19 vaccine confers protection from SARS-COV-2 challenge in rhesus macaques. *Nat. Commun.* **11**, 4207 (2020).
44. van Doremalen, N. et al. Intranasal ChAdOx1 nCoV-19/AZD1222 vaccination reduces viral shedding after SARS-CoV-2 D614G challenge in preclinical models. *Sci. Transl. Med.* **13**, https://doi.org/10.1126/scitranslmed.abh0755 (2021).
45. Hassan, A. O. et al. A single intranasal dose of chimpanzee adenovirus-vectored vaccine protects against SARS-CoV-2 infection in rhesus macaques. *Cell Rep. Med* **2**, 100230 (2021).
46. Costa Clemens, S. A. et al. Heterologous versus homologous COVID-19 booster vaccination in previous recipients of two doses of CoronaVac COVID-19 vaccine in Brazil (RHH-001): a phase 4, non-inferiority, single blind, randomised study. *Lancet* **399**, 521–529 (2022).
47. Cao, Y. et al. Humoral immunogenicity and reactogenicity of CoronaVac or ZF2001 booster after two doses of inactivated vaccine. *Cell Res* **32**, 107–109 (2022).
48. Li, J. et al. Heterologous AD5-nCOV plus CoronaVac versus homologous CoronaVac vaccination: a randomized phase 4 trial. *Nat. Med* **28**, 401–409 (2022).
49. Moss, P. The T cell immune response against SARS-CoV-2. *Nat. Immunol.* **23**, 186–193 (2022).

Acknowledgements

We thank Prof. Alain Townsend (Oxford University) for providing helpful discussion. This work was supported by the National Natural Science Foundation of China (82471856, J.H.) and the National Key R&D Program (2023YFC2307800). All animal experiments were performed in animal facilities under specific pathogen-free conditions.

Author contributions

J.H. conceived the study. J.H., H.D., E.F., D.S., J.X.Z., J.C.Z., S.L. and X.P. supervised the study and designed the experiments. Y.Z., H.R., X.H. Y.L. and R.G. prepared the vaccine and vaccination of animals. Y.Z. and H.R. performed pseudovirus neutralization and flow cytometry experiments. Y.Z., Z.Z., J.S. and Y.Y. performed live SARS-CoV-2 neutralization assay, SARS-CoV-2 challenge in mice and determined the viral loads. Y.W. performed the experiments related to the hamster transmission model. M.Z. performed the Ex vivo fluorescent imaging experiments. J.H. wrote the initial manuscript draft, with the other authors providing editorial comments. All authors reviewed the manuscript.

Competing interests

The authors declare no competing interests.

Additional information

Supplementary information The online version contains supplementary material available at https://doi.org/10.1038/s41541-025-01155-4.

Correspondence and requests for materials should be addressed to XiaoYan Pan, Shu-Lin Liu, Jincun Zhao or Jiandong Huo.